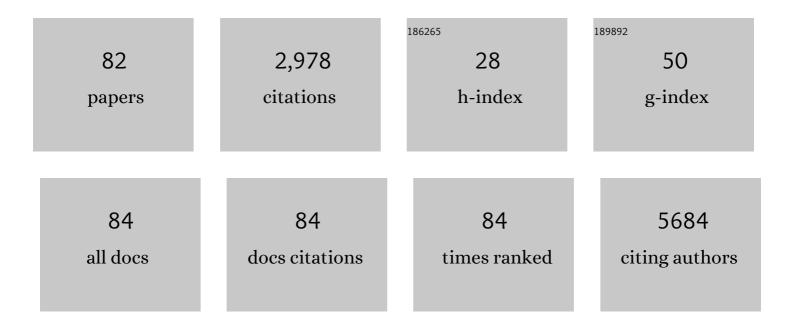
Stephen J Sawiak

List of Publications by Year in descending order

Source: https://exaly.com/author-pdf/9197436/publications.pdf Version: 2024-02-01



#	Article	IF	CITATIONS
1	Higher-order brain regions show shifts in structural covariance in adolescent marmosets. Cerebral Cortex, 2022, 32, 4128-4140.	2.9	3
2	Cholangiocyte organoids can repair bile ducts after transplantation in the human liver. Science, 2021, 371, 839-846.	12.6	170
3	MRI-guided histology of TDP-43 knock-in mice implicates parvalbumin interneuron loss, impaired neurogenesis and aberrant neurodevelopment in amyotrophic lateral sclerosis-frontotemporal dementia. Brain Communications, 2021, 3, fcab114.	3.3	11
4	U-net model for brain extraction: Trained on humans for transfer to non-human primates. NeuroImage, 2021, 235, 118001.	4.2	42
5	Over-activation of primate subgenual cingulate cortex enhances the cardiovascular, behavioral and neural responses to threat. Nature Communications, 2020, 11, 5386.	12.8	56
6	latrogenic transmission of Alzheimer's disease: Evidence based on experimental inoculation of Alzheimer's disease: Alzheimer's and Dementia, 2020, 16, e042957.	0.8	1
7	Accelerating the Evolution of Nonhuman Primate Neuroimaging. Neuron, 2020, 105, 600-603.	8.1	92
8	Insula serotonin 2A receptor binding and gene expression contribute to serotonin transporter polymorphism anxious phenotype in primates. Proceedings of the National Academy of Sciences of the United States of America, 2019, 116, 14761-14768.	7.1	20
9	Encephalopathy induced by Alzheimer brain inoculation in a non-human primate. Acta Neuropathologica Communications, 2019, 7, 126.	5.2	33
10	A novel cyclic biased agonist of the apelin receptor, MM07, is disease modifying in the rat monocrotaline model of pulmonary arterial hypertension. British Journal of Pharmacology, 2019, 176, 1206-1221.	5.4	32
11	Fractionating Blunted Reward Processing Characteristic of Anhedonia by Over-Activating Primate Subgenual Anterior Cingulate Cortex. Neuron, 2019, 101, 307-320.e6.	8.1	92
12	Trajectories and Milestones of Cortical and Subcortical Development of the Marmoset Brain From Infancy to Adulthood. Cerebral Cortex, 2018, 28, 4440-4453.	2.9	48
13	Elabela/Toddler Is an Endogenous Agonist of the Apelin APJ Receptor in the Adult Cardiovascular System, and Exogenous Administration of the Peptide Compensates for the Downregulation of Its Expression in Pulmonary Arterial Hypertension. Circulation, 2017, 135, 1160-1173.	1.6	183
14	Brain hypoxia mapping in acute stroke: Back-to-back T2′ MR versus ¹⁸ F-fluoromisonidazole PET in rodents. International Journal of Stroke, 2017, 12, 752-760.	5.9	10
15	Evolution of structural abnormalities in the rat brain following in utero exposure to maternal immune activation: A longitudinal in vivo MRI study. Brain, Behavior, and Immunity, 2017, 63, 50-59.	4.1	64
16	In vivo magnetic resonance images reveal neuroanatomical sex differences through the application of voxel-based morphometry in C57BL/6 mice. NeuroImage, 2017, 163, 197-205.	4.2	29
17	Behavior of Supramolecular Assemblies of Radiometal-Filled and Fluorescent Carbon Nanocapsules InÂVitro and InÂVivo. CheM, 2017, 3, 437-460.	11.7	22
18	Converging Prefronto-Insula-Amygdala Pathways in Negative Emotion Regulation inÂMarmoset Monkeys. Biological Psychiatry, 2017, 82, 895-903.	1.3	27

#	Article	IF	CITATIONS
19	Reconstruction of the mouse extrahepatic biliary tree using primary human extrahepatic cholangiocyte organoids. Nature Medicine, 2017, 23, 954-963.	30.7	210
20	Effects of hyperoxia on 18F-fluoro-misonidazole brain uptake and tissue oxygen tension following middle cerebral artery occlusion in rodents: Pilot studies. PLoS ONE, 2017, 12, e0187087.	2.5	3
21	Similar Progression of Morphological andÂMetabolic Phenotype in R6/2 Mice with Different CAG Repeats Revealed by In Vivo Magnetic Resonance Imaging and Spectroscopy. Journal of Huntington's Disease, 2016, 5, 271-283.	1.9	1
22	In vivo γâ€aminobutyric acid measurement in rats with spectral editing at 4.7T. Journal of Magnetic Resonance Imaging, 2016, 43, 1308-1312.	3.4	16
23	MR fingerprinting with simultaneous B1 estimation. Magnetic Resonance in Medicine, 2016, 76, 1127-1135.	3.0	124
24	Additional sampling directions improve detection range of wireless radiofrequency probes. Magnetic Resonance in Medicine, 2016, 76, 913-918.	3.0	0
25	An EEG Investigation of Sleep Homeostasis in Healthy and CLN5 Batten Disease Affected Sheep. Journal of Neuroscience, 2016, 36, 8238-8249.	3.6	27
26	BCL11A Haploinsufficiency Causes an Intellectual Disability Syndrome and Dysregulates Transcription. American Journal of Human Genetics, 2016, 99, 253-274.	6.2	118
27	O4â€1 1â€03: First Demonstration of Functional and Morphological Alterations in Primates after Alzheimer Brain Homogenates Inoculation. Alzheimer's and Dementia, 2016, 12, P360.	0.8	0
28	Normobaric hyperoxia markedly reduces brain damage and sensorimotor deficits following brief focal ischaemia. Brain, 2016, 139, 751-764.	7.6	31
29	Impulsivity is predicted by the thinness of the insular cortex in rats. Molecular Psychiatry, 2016, 21, 445-445.	7.9	7
30	Direct Evaluation of MR-Derived Attenuation Correction Maps for PET/MR of the Mouse Myocardium. IEEE Transactions on Nuclear Science, 2016, 63, 195-202.	2.0	1
31	From impulses to maladaptive actions: the insula is a neurobiological gate for the development of compulsive behavior. Molecular Psychiatry, 2016, 21, 491-499.	7.9	88
32	The Cambridge MRI database for animal models of Huntington disease. NeuroImage, 2016, 124, 1260-1262.	4.2	4
33	Molecular neuropathology of the synapse in sheep with <scp>CLN</scp> 5 Batten disease. Brain and Behavior, 2015, 5, e00401.	2.2	28
34	Cerebrovascular and blood–brain barrier impairments in Huntington's disease: Potential implications for its pathophysiology. Annals of Neurology, 2015, 78, 160-177.	5.3	204
35	What is the Optimal Duration of Middle-Cerebral Artery Occlusion Consistently Resulting in Isolated Cortical Selective Neuronal Loss in the Spontaneously Hypertensive Rat?. Frontiers in Neurology, 2015, 6, 64.	2.4	11
36	Rapid and Progressive Regional Brain Atrophy in CLN6 Batten Disease Affected Sheep Measured with Longitudinal Magnetic Resonance Imaging. PLoS ONE, 2015, 10, e0132331.	2.5	20

#	Article	IF	CITATIONS
37	Dissociable Rate-Dependent Effects of Oral Methylphenidate on Impulsivity and D _{2/3} Receptor Availability in the Striatum. Journal of Neuroscience, 2015, 35, 3747-3755.	3.6	54
38	Impaired Limbic Cortico-Striatal Structure and Sustained Visual Attention in a Rodent Model of Schizophrenia. International Journal of Neuropsychopharmacology, 2015, 18, pyu010-pyu010.	2.1	28
39	Cortical Selective Neuronal Loss, Impaired Behavior, and Normal Magnetic Resonance Imaging in a New Rat Model of True Transient Ischemic Attacks. Stroke, 2015, 46, 1084-1092.	2.0	26
40	A survey of patient motion in disorders of consciousness and optimization of its retrospective correction. Magnetic Resonance Imaging, 2015, 33, 346-350.	1.8	8
41	Combining MRI With PET for Partial Volume Correction Improves Image-Derived Input Functions in Mice. IEEE Transactions on Nuclear Science, 2015, 62, 628-633.	2.0	3
42	Serotonergic, Brain Volume and Attentional Correlates of Trait Anxiety in Primates. Neuropsychopharmacology, 2015, 40, 1395-1404.	5.4	18
43	Complex I Deficiency Due to Selective Loss of Ndufs4 in the Mouse Heart Results in Severe Hypertrophic Cardiomyopathy. PLoS ONE, 2014, 9, e94157.	2.5	41
44	Voxel-based morphometry analyses of in vivo MRI in the aging mouse lemur primate. Frontiers in Aging Neuroscience, 2014, 6, 82.	3.4	32
45	Right Ventricular Dysfunction in the R6/2 Transgenic Mouse Model of Huntington's Disease is Unmasked by Dobutamine. Journal of Huntington's Disease, 2014, 3, 25-32.	1.9	17
46	Orbitofrontal Dopamine Depletion Upregulates Caudate Dopamine and Alters Behavior via Changes in Reinforcement Sensitivity. Journal of Neuroscience, 2014, 34, 7663-7676.	3.6	50
47	Functional assessment of the mouse heart by MRI with a 1-min acquisition. NMR in Biomedicine, 2014, 27, 733-737.	2.8	10
48	Brain γâ€∎minobutyric acid: a neglected role in impulsivity. European Journal of Neuroscience, 2014, 39, 1921-1932.	2.6	52
49	Gamma Aminobutyric Acidergic and Neuronal Structural Markers in the Nucleus Accumbens Core Underlie Trait-like Impulsive Behavior. Biological Psychiatry, 2014, 75, 115-123.	1.3	81
50	Trajectory correction for free-breathing radial cine MRI. Magnetic Resonance Imaging, 2014, 32, 961-964.	1.8	11
51	Comparison of first pass bolus AIFs extracted from sequential 18F-FDG PET and DSC-MRI of mice. Nuclear Instruments and Methods in Physics Research, Section A: Accelerators, Spectrometers, Detectors and Associated Equipment, 2014, 734, 137-140.	1.6	3
52	Mitochondria selective S â€nitrosation by mitochondriaâ€targeted S â€nitrosothiol protects against postâ€infarct heart failure in mouse hearts. European Journal of Heart Failure, 2014, 16, 712-717.	7.1	39
53	Early and progressive circadian abnormalities in Huntington's disease sheep are unmasked by social environment. Human Molecular Genetics, 2014, 23, 3375-3383.	2.9	78
54	Combining MRI with PET for partial volume correction improves image-derived input functions in mice. EJNMMI Physics, 2014, 1, A84.	2.7	1

#	Article	IF	CITATIONS
55	Direct evaluation of MR-derived attenuation correction maps for PET/MR of the mouse myocardium. EJNMMI Physics, 2014, 1, A85.	2.7	Ο
56	Comparison of MR-based attenuation correction and CT-based attenuation correction of whole-body PET/MR imaging. European Journal of Nuclear Medicine and Molecular Imaging, 2014, 41, 1574-1584.	6.4	41
57	PET/MRI assessment of the infarcted mouse heart. Nuclear Instruments and Methods in Physics Research, Section A: Accelerators, Spectrometers, Detectors and Associated Equipment, 2014, 734, 152-155.	1.6	6
58	Voxel-based morphometry with templates and validation in a mouse model of Huntington's disease. Magnetic Resonance Imaging, 2013, 31, 1522-1531.	1.8	62
59	Characterizing infarction and selective neuronal loss following temporary focal cerebral ischemia in the rat: A multi-modality imaging study. Neurobiology of Disease, 2013, 51, 120-132.	4.4	38
60	MRI-derived arterial input functions for PET kinetic modelling in rats. Nuclear Instruments and Methods in Physics Research, Section A: Accelerators, Spectrometers, Detectors and Associated Equipment, 2013, 702, 126-128.	1.6	3
61	PET/MRI in the infarcted mouse heart with the Cambridge split magnet. Nuclear Instruments and Methods in Physics Research, Section A: Accelerators, Spectrometers, Detectors and Associated Equipment, 2013, 702, 47-49.	1.6	6
62	A comparison of four PET tracers for brain hypoxia mapping in a rodent model of stroke. Nuclear Medicine and Biology, 2013, 40, 338-344.	0.6	15
63	Reliability of using a fixed matrix in coregistration of combined PET–MRI in a split magnet design. Nuclear Instruments and Methods in Physics Research, Section A: Accelerators, Spectrometers, Detectors and Associated Equipment, 2013, 702, 54-55.	1.6	2
64	Translating positron emission tomography studies in animals to stimulant addiction: promises and pitfalls. Current Opinion in Neurobiology, 2013, 23, 597-606.	4.2	7
65	A fast protocol for infarct quantification in mice. Journal of Magnetic Resonance Imaging, 2013, 38, 468-473.	3.4	12
66	Baseline-Dependent Effects of Cocaine Pre-Exposure on Impulsivity and D2/3 Receptor Availability in the Rat Striatum: Possible Relevance to the Attention-Deficit Hyperactivity Syndrome. Neuropsychopharmacology, 2013, 38, 1460-1471.	5.4	48
67	MRI and PET in Mouse Models of Myocardial Infarction. Journal of Visualized Experiments, 2013, , e50806.	0.3	8
68	B.6 - GABA-ERGIC AND NEURONAL STRUCTURAL MARKERS IN THE NUCLEUS ACCUMBENS CORE PREDICT TRAIT-LIKE IMPULSIVITY IN RATS. Behavioural Pharmacology, 2013, 24, e27-e28.	1.7	0
69	Riociguat Reduces Infarct Size and Post-Infarct Heart Failure in Mouse Hearts: Insights from MRI/PET Imaging. PLoS ONE, 2013, 8, e83910.	2.5	36
70	A fast surface-aware 3D non-linear image registration algorithm implemented on a GPU. , 2012, , .		0
71	24â€Initial Results of Simultaneous PET/MRI Evaluation of the Infarcted Mouse Heart. Heart, 2012, 98, A7.4-A8.	2.9	0
72	07â€Simultaneous Positron Emission Tomography and Magnetic Resonance Imaging of Receptors Using a Novel Combined Pre-Clinical Micropet/Mr System. Heart, 2012, 98, A2.4-A3.	2.9	0

#	Article	IF	CITATIONS
73	Tensor-Based Morphometry and Stereology Reveal Brain Pathology in the Complexin1 Knockout Mouse. PLoS ONE, 2012, 7, e32636.	2.5	21
74	Direct Evidence of Progressive Cardiac Dysfunction in a Transgenic Mouse Model of Huntington's Disease. Journal of Huntington's Disease, 2012, 1, 57-64.	1.9	31
75	Huntington's Disease Mouse Models Online: High-Resolution MRI Images with Stereotaxic Templates for Computational Neuroanatomy. PLoS ONE, 2012, 7, e53361.	2.5	9
76	3000 non-rigid medical image registrations overnight on a single PC. , 2011, , .		5
77	Validation and Quantification of [¹⁸ F]Altanserin Binding in the Rat Brain Using Blood Input and Reference Tissue Modeling. Journal of Cerebral Blood Flow and Metabolism, 2011, 31, 2334-2342.	4.3	21
78	Radiofrequency coil design for simultaneous PET/MR systems. , 2010, , .		5
79	Exceptionally fast non-linear 3D image registration using GPUs. , 2009, , .		9
80	Exceptionally fast non-linear 3D image registration using GPUs. , 2009, , .		3
81	Voxel-based morphometry in the R6/2 transgenic mouse reveals differences between genotypes not seen with manual 2D morphometry. Neurobiology of Disease, 2009, 33, 20-27.	4.4	140
82	Use of magnetic resonance imaging for anatomical phenotyping of the R6/2 mouse model of Huntington's disease. Neurobiology of Disease, 2009, 33, 12-19.	4.4	63